Research Article

Synthesis and characterization of NiO nanoparticles by chemical as well as green routes and their comparisons with respect to cytotoxic effect and toxicity studies in microbial and MCF-7 cancer cell models

SN

P. Vijaya Kumar[1] · A. Jafar Ahamed[2] · M. Karthikeyan[3]

Abstract

This contribution reports on the synthesis and also compares the main physical properties of nickel oxide nanoparticles (NiO NPs) synthesized by a completely green process using *Gymnema sylvestere* plant extract and sodium hydroxide as an effective reducing agent for co-precipitation method. The synthesized nanoparticles were characterized by XRD, HRTEM, EDS, FTIR, UV–visible, XPS, EPR and zeta potential analysis methods. Further the synthesized NiO NPs were evaluated the in vitro toxicity studies using microbial and MCF-7 cancer cell line models. Further cytotoxicity studies and acridine orange and ethidium bromide staining confirmed that green synthesized NiO NPs possess low toxicity compared with chemically synthesized NiO NPs.

Keywords NiO nanoparticles · Physical properties · *Gymnema sylvestere* · Cytotoxicity

1 Introduction

Man-made materials and nanoparticles are being rapidly produced in large quantities throughout the world [1]. Many studies conducted in the past few decades suggest that nanomaterials have different toxicity profiles compared with larger particles because of their small size and high reactivity. In our daily life, more and more nanomaterials are introduced due their wide spread applications. But their adverse effects to the environmental and human health are a major concern [2]. Meanwhile, owing to their size and unusual properties, nanoparticles can enter the body and cross biological barriers relatively unimpeded. Several studies have reported that nanoparticles enter the body through the respiratory tract and can penetrate the pulmonary epithelium; they can reach the interstitium and be deposited in the peripheral lung tissue [3, 4]. Since insoluble metal oxide nanomaterials are expected to be more environmentally persistent, investigations on environmental perseverance, bioaccumulation and toxicity of these nanomaterials help to assess the potential risks and provide information to industry to develop safer nanomaterials [5, 6].

Owing to their specific functional characteristics and importance in a wide variety of technical applications, nickel oxide (NiO) is extensively investigated as electronic component, ceramic materials and catalysts. It is also known that nickel compounds (including NiO) have harmful effects. Nickel compounds are classified as class I carcinogenic material by the International Agency for Research on Cancer (IARC Monographs on the evaluation of Carcinogenic Risks to Human, Volume 49, 1990). In general, NiO is classified as having relatively lower toxicity than other nickel compounds [7, 8].

Recent studies indicate the great potential of NiO NPs in biomedical applications, including cancer diagnosis and therapy. Mariam et al. [9] reported that Ni and NiO NPs used to study the cytotoxic effect against for human

✉ P. Vijaya Kumar, pdvijayjmc@gmail.com | [1]Department of Chemistry, Jairams Arts and Science College, Karur, Tamil Nadu 639 003, India. [2]Post Graduate and Research Department of Chemistry, Jamal Mohamed College (Autonomous), Tiruchirappalli, Tamil Nadu 620 020, India. [3]Department of Chemistry, Periyar Maniammai Institute of Arts and Science, Vallam, Thanjavur, Tamil Nadu 613 403, India.

colon adenocarcinoma (HT-29) cells. Adam et al. [10] have investigated the cytotoxicity and apoptotic effects of NiO NPs on human cervix epithelioid carcinoma (HeLa) cell line. Ahamed et al. [11] have been studied the NiO NPs exert cytotoxicity via oxidative stress and induce apoptotic response in human liver (HepG2) cancer cells. Duan et al. [12] reported that the NiO NPs induce apoptosis through repressing SIRT1 in human bronchial epithelial cancer cells. Ramasami et al. [13] investigated antimicrobial activity against the two bacterial (*Bacillus cereus* and *Klebsiella aerogenes*) strains and one fungal (*Candida albicans*) treated with NiO NPs. Talebian et al. [14] tested the antibacterial activity of NiO NPs against two common food borne pathogenic bacteria *Stapylococcus aureus* and *Escherichia coli*.

However, variations observed in the biological responses of metal oxide nanoparticles could be due to the differences in the ability to produce the reactive oxygen species (ROS) and their types. Apart from this, the physico-chemical properties (size, shape, surface area, surface coating, composition and dissolution) of metal oxide nanoparticles, method of synthesis, as well as impurities play a major role in their biological outcomes [15]. We have synthesised NiO nanoparticles in chemical and green synthesis method. Moreover, there was no literature found in the synthesis of NiO NPs using *Gymnema sylvestre* plant extracts.

The synthesised nanoparticles were characterized by X-ray diffraction studies (XRD), Fourier transform infra-red spectroscopy (FTIR), high resolution transmission electron microscopy (HRTEM) with selected area diffraction studies (SAED) and energy dispersive analysis (EDAX), UV–visible spectroscopy, photoluminescence (PL) studies, X-ray photoelectron spectroscopy (XPS), electron paramagnetic resonance (EPR) spectroscopy and zeta potential analysis. To the best of our knowledge, this is the first report for the comparative toxicity studies of chemical and green synthesised (*G. sylvestre* plant extract reduced) NiO NPs in bacterial and MCF 7 cancer cells.

2 Experimental methods

2.1 Synthesis of NiO NPs using *G. sylvestre* leaves extract

15 g of finely chopped *G. Sylvestre* leaves were weighed. Then, 150 ml of double distilled water was added and boiled at 60 °C for 15 min. The obtained extract was filtered using Whatman no. 1 filter paper and the filtrate was collected in a 250 ml Erlenmeyer flask. Thereafter, 0.1 M nickel nitrate hexahydrate ($Ni(NO_3)_2 \cdot 6H_2O$) solution was added into 150 ml of *G. sylvestre* leaves extract and it was stirred constantly at

80 °C for 6 h. A black colour precipitate was obtained. Further, the precipitate was dried at 120 °C for 6 h. The obtained NiO nanopowder was calcined at 600 °C for 5 h.

2.2 Synthesis of NiO NPs by co-precipitation method

In this typical chemical synthesis of NiO NPs, the following high purity chemicals such as, $Ni(NO_3)_2 \cdot 6H_2O$ and sodium hydroxide (NaOH) were used as the precursors without further purification. Required amount of $Ni(NO_3)_2 \cdot 6H_2O$ (0.1 M) was completely dissolved in deionized water, aqueous NaOH (0.8 M) solution was added drop wise to the aqueous nickel nitrate and this solution was stirred at 80 °C for 6 h. A green colour precipitate was formed slowly, which was washed several times with double distilled water and ethanol. The precipitate was dried at 120 °C. The NiO NPs thus obtained were annealed at 600 °C for 5 h. Finally, black colour NiO NPs was collected and used for further studies.

2.3 Antimicrobial activity of NiO NPs

Antimicrobial activity of the green and chemically synthesized NiO NPs was carried out by agar well diffusion method against two pathogenic bacterial strains namely *S. aureus* (gram positive) and *E. coli* (gram negative) on Muller-Hinton agar, according to the guidelines of Clinical and Laboratory Standards Institute (CLSI) [16]. The media plates (MHA) were streaked with bacteria for 2–3 times by rotating the plate at 60° angle for each streak to ensure homogeneous distribution of the inoculums. Then the agar plates were swabbed with 100 ml each of overnight cultures of *S. aureus* and *E. coli* using a sterile L-shaped glass rod. Using a sterile cork-borer, wells (6 mm) were created in each petri plate. Varied concentrations of NiO NPs (1 µg/ml, 3 µg/ml and 5 µg/ml for both G+ and G− bacteria) were loaded onto the petri plates followed by incubation for 24 h at 37 °C for bacteria. After the incubation period, the diameter of the zone of inhibition (DZI) was recorded. Kanamycin (Hi-Media) was used as the positive control against gram negative and gram positive bacteria to compare the efficacy of the test samples. We have simultaneously studied whether the dimethyl sulfoxide (DMSO) without the NiO NPs plays any active role as a biocide or not. As there is no any disc zone of inhibition observed, it confirms that DMSO doesn't show any biocidal property.

2.4 Anticancer activity

2.4.1 Cell culture

The MCF-7 breast adenocarcinoma cancer cells were cultured in RPMI 1640 medium (Sigma-Aldrich, St. Louis, MO,

USA), supplemented with 10% fetal bovine serum (Sigma, USA) and 10,000 IU penicillin and 100 µg/ml of streptomycin as antibiotics (Himedia, Mumbai, India), in 96 well culture plates, at 37 °C, in a humidified atmosphere of 5% CO_2, in a CO_2 incubator (Forma, Thermo Scientific, USA). All experiments were performed using cells from passage 15 or less.

2.4.2 MTT assay

The green and chemically synthesized NiO NPs were suspended in DMSO, diluted in culture medium and used to treat the chosen cell line (MCF-7) over a complex concentration range of 5–100 µg/ml for 24 h. DMSO solution was used as the solvent control. A miniaturized viability assay using 3-(4,5-di-methylthiazol-2-yl)-2,5-diphenyl-2H-tetrazolium bromide (MTT) was carried out [17]. To each well, 20 µl of 5 µg/ml MTT in phosphate buffer (PBS) was added. The plates were wrapped with aluminium foil and incubated for 4 h at 37 °C. The purple formazan product was dissolved by the addition of 100 µl of 100% DMSO to each well. The absorbance was monitored at 570 nm (measurement) and 630 nm (reference) using a 96 well plate reader (Biorad 680). The data were collected for four replicates. The percentage of inhibition was calculated from this data using the formula

$$\% \text{ of inhibition} = \frac{\text{mean OD of untreated cells (control)} - \text{mean OD of treated cells}}{\text{mean OD of untreated cells (control)}} \times 100$$

2.4.3 Acridine orange (AO) and ethidium bromide (EB) staining

AO/EB staining was performed as described by Spector et al. [18]. The cell suspension of each sample containing 30,000 cells/ml cells, was treated with 200 µl of AO/EB solution (100 µl/mg AO and 100 µl/mg EB in PBS) and examined by a Olympus inverted fluorescence microscope (Ti-Eclipse) using an UV filter (450–490 nm). One hundred cells per sample were counted in tetraplicate for each dose point. The cells were scored as viable, apoptotic or necrotic as judged by the fluorescence emittance, nuclear morphology and membrane integrity [18]. The morphological changes were also observed and photographed.

3 Characterization techniques

The NiO NPs were characterized by X-ray diffractometer (model: X'PERT PRO PAN analytical). The diffraction pattern was recorded in the range of 25°–80° for the NiO

NPs, at the monochromatic wavelength of 1.54 Å. The morphology of the synthesized NiO NPs was examined using HRTEM. Sample for HRTEM analysis was prepared by drop coating the NPs solutions on carbon-coated copper grids at room temperature. The excess NPs solutions were removed with filter paper. The copper grid was finally dried at room temperature and was subjected to TEM analysis by the instrument Tecnai F20 model operated at an accelerating voltage of 200 kV. The NiO NPs were analyzed by EDAX (model: ULTRA 55). The FT-IR spectrum was recorded in the range of 400–4000 cm^{-1} by using Perkin-Elmer spectrometer. Ultraviolet–visible (UV–Vis) spectra of NiO nanoparticles were recorded on a Perkin-Elmer UV-Lambda 25 spectrophotometer (Perkin-Elmer, Norwalk, Connecticut). The PL emission study of the sample was carried out using Horiba Jobin–YVON spectrofluorometer (model: FLUORO-MAX-4, 450 W high pressure xenon lamp as the excitation source, photomultiplier at a range 325–550 nm). The XPS measurements were performed with an XPS instrument (Carl Zeiss) under ultra-high vacuum with Al K_α excitation at 250 W. To obtain information on defects and vacancies, EPR was recorded using X-band JEOL JES-RE1X at room temperature. Zeta potential measurement was carried out by using Malvern Zetasizer instrument.

4 Results and discussion

4.1 X-ray diffraction studies

The X-ray diffraction patterns of green and chemically synthesised NiO NPs are shown in Fig. 1a. The XRD result shows that all the samples have cubic nickel oxide (ICDD:78-0643) belonging to the *Fm3m* space group. Figure 1b shows that enlarged peak position of green and chemically synthesized NiO NPs. As compared to the green synthesized NiO NPs, the intensity of chemically synthesized NiO NPs increase because the energy from the heat can enhance the vibration and diffusion of the lattice atoms for crystallization. The peaks are located at an angle of 2θ at 37.2685, 43.5040, 63.0885, 75.3950 and 79.5011 for green synthesised NiO NPs and 37.2826, 43.3037, 62.9345, 75.3463 and 79.4478 for chemically synthesised NiO NPs which correspond to the (111), (200), (220), (311) and (222) plane of the cubic structure for green synthesized NiO and chemically synthesized NiO NPs respectively.
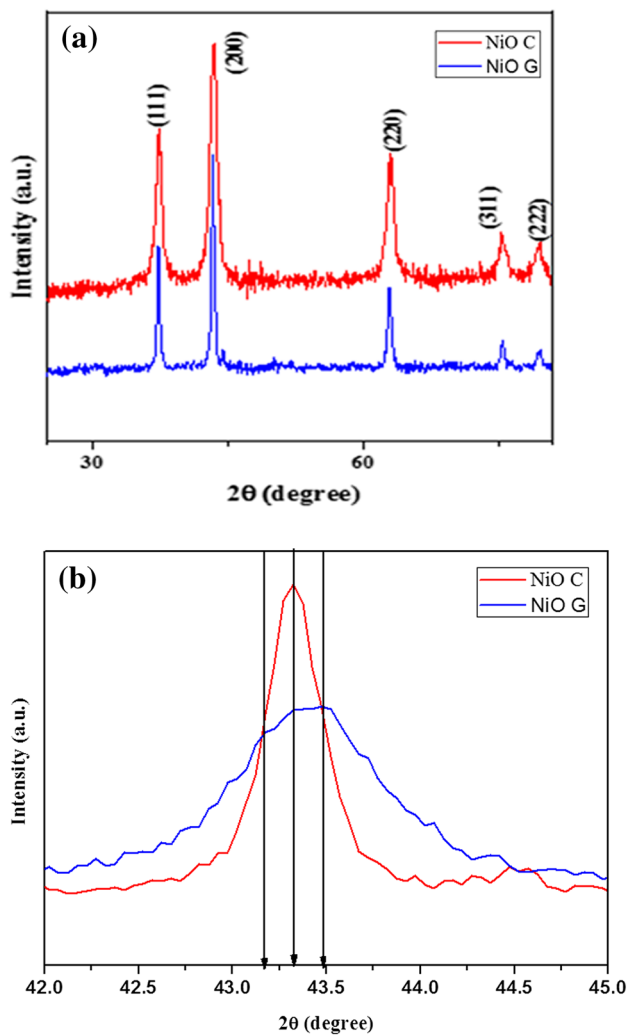
Fig. 1 **a** X-ray powder diffraction patterns of green and chemically synthesised NiO NPs, **b** an enlarged version of the XRD pattern of NiO NPs between 35.4° and 38.7°

The lattice constants 'a' of the *cubic structure* of NiO can be calculated by using the relation

$$\frac{1}{d^2} = \left(\frac{h^2 + k^2 + l^2}{a^2} \right) \tag{1}$$

Or

$$a = \sqrt{d^2 \left(h^2 + k^2 + l^2 \right)} \tag{2}$$

The unit cell volume is calculated by the relation $V = a^3$. The calculated lattice constant value and unit cell volume are presented in Table 1.

The average crystallite size of the samples are calculated by Debye–Scherrer's relation

$$\text{Average crystalline size D} = \frac{k\lambda}{\beta_{D}\cos\theta} \tag{3}$$

where λ—the wavelength of the radiation (1.54056 Å for Cu Kα radiation), k—a constant which is equal to 0.94, β—the peak width at half-maximum intensity, θ—the peak position. The average crystallite size is found to be 23 nm and 32 nm for chemical and green synthesised NiO NPs respectively. The average crystallite size decreases in the Chemical synthesised NiO NPs. The reduction in the particle size is mainly due to the temperature effect. Further, micro strain (ε) was estimated by the following relations [18]

$$\varepsilon = \frac{\beta\cos\theta}{4} \tag{4}$$

The micro-strain increases in the case of chemically synthesized NiO NPs as compared to that of green synthesized NiO NPs. It is evident that the increase in strain causes the increase in the lattice constant values, reduction in the particles size, the broadening and small shifts in the XRD peaks (Table 2).

4.2 Functional group analysis

The FTIR spectra of green and chemically synthesized NiO NPs are shown in Fig. 2. The broad absorption band located at 3441 and 3323 cm^{-1} are attributed the O–H stretching vibration of interlayer water molecules and H-bound to OH group for both NiO NPs respectively. The peaks at 2915 cm^{-1} are due to asymmetric stretching (C–H) mode of the CH_2 groups for green synthesized NiO NPs [19]. The band at 2123 cm^{-1} is attributed to the C–H stretching vibrations are NiO NPs. The absorption peaks at 1643 cm^{-1} and 1656 cm^{-1} are due to the bending mode (H–O–H) of the water molecule of green synthesized NiO and chemically synthesized NiO NPs respectively. C–H bending vibrations are located at 1026 cm^{-1} and 1118 cm^{-1} for both NiO NPs respectively. The strong band at 423 and 436 cm^{-1}

Table 1 X-ray diffraction parameter values of the green and chemically synthesised NiO NPs

Sample	Lattice parameter values (Å) A	Volume V (Å)³	Average crystalline size D (nm)	Micro-strain ε
NiO green	4.1605	72.0172	27	0.01814
NiO chem	4.1787	72.9665	13	0.03613

Table 2 FTIR peaks assignments of green and chemically synthesised NiO NPs [19, 20]

Sl. no.	NiO (green)	NiO (chem)	Assignment
1	3441	3323	OH stretching
2	2915	2123	C–H stretching
3	1643	1656	C–H stretching
5	1380	1394	H–O–H bending
6	1026	1118	CH bending
7	423	436	Ni–O stretching
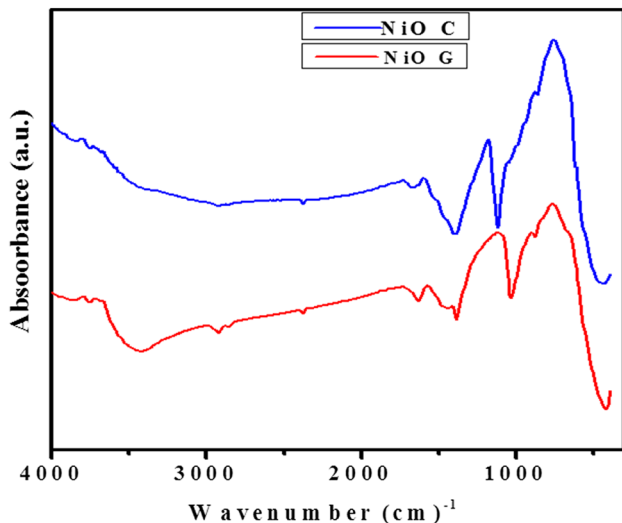
Fig. 2 FTIR spectra of the green and chemically synthesised NiO NPs

correspond to the Ni–O starching for green synthesized NiO and chemically synthesized NiO NPs [20].

4.3 Morphological analysis

In order to predict the morphology and size of the green and chemically synthesised NiO NPs, HRTEM images have been recorded as shown in Fig. 3a, b. It can be clearly observed that the synthesised product consist of nearly cube shaped particles with size around 10–20 nm. It is in good agreement with an average crystallite size obtained from Scherrer's formula. Selected area diffraction pattern (SAED) originated from the NiO nanoparticles are shown in the Fig. 3c, d. The appearance of strong diffraction spots rather than diffraction rings confirmed the formation of single crystalline cubic nickel oxide.

4.4 Elemental analysis

The quantitative chemical compositional analyses of green and chemically synthesised NiO samples were carried out using EDAX. The typical EDAX spectra of the synthesized NiO NPs are shown in Fig. 4a, b. It revealed that the presence of Ni and O in chemically synthesized NPs is found to be 43.58 and 56.42% respectively. Likewise, the composition of Ni and O in the green synthesized sample is found to be 43.55% and 56.45% respectively. Moreover, no additional peaks corresponding to any other elements except Ni and O were observed.

4.5 Optical studies

UV–visible optical absorption spectra of green and chemically synthesised NiO NPs were recorded at room temperature in the wavelength range 350–800 nm as shown in Fig. 5. The samples were uniformly dispersed in distilled water, followed by ultra sonification for 15–20 min before recording UV–Vis spectra. Blue shift in the absorption edge is observed in the chemically synthesised NPs (243 nm) compared with green synthesised NiO NPs (259 nm). This is assigned to the intrinsic band gap absorption. These peaks are due to the electronic transition occurring between the valence band and the conduction band [21].

The direct band gap energy was calculated by using Tauc relation as given below.

$$\alpha h\upsilon = A\left(h\upsilon - E_g\right)^n \tag{5}$$

where E_g is the optical band gap, α is the absorption coefficient, A is a constant and the exponent n depends on the transition. Considering direct band transition in NiO NPs, a plot between $(\alpha h\upsilon)^2$ versus photon energy ($h\upsilon$) is drawn for green and chemically synthesized NiO NPs as shown in Fig. 6. The intercept of the tangent to the plot on the X-axis gives the direct band gap of NiO NPs. The optical band gap values obtained from Fig. 6 are 5.1 and 4.78 eV respectively for the chemical and green synthesised NiO NPs samples. The optical band gap of NiO in the present study is higher than the bulk value (3.65 eV). It is due to the quantum confinement effect. This effect is due the chemical defects or vacancies present in the intergranular regions generating new energy level to increase the band gap energy [22, 23].

4.6 Photoluminescence (PL) studies

PL study is one of the important method to investigate the structural defects such as oxygen vacancies and quantum size effects. Figure 7 depicts the PL spectra
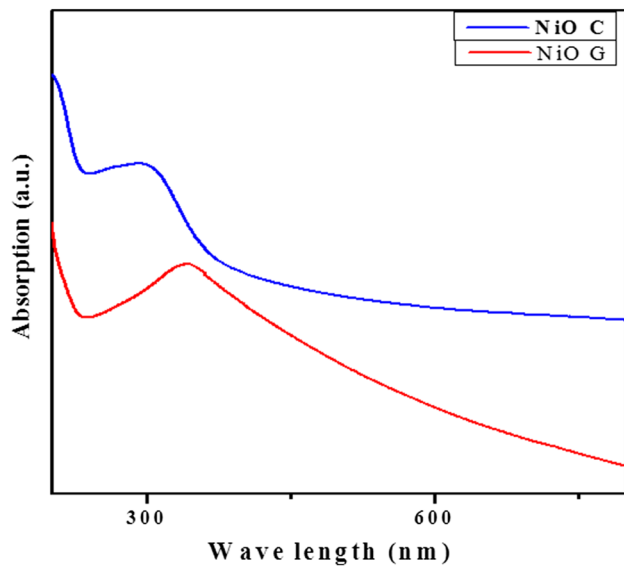
Fig. 3 **a**, **b** HRTEM image of green and chemically synthesised NiO NPs, **c**, **d** SAED pattern of green and chemically synthesised NiO NPs
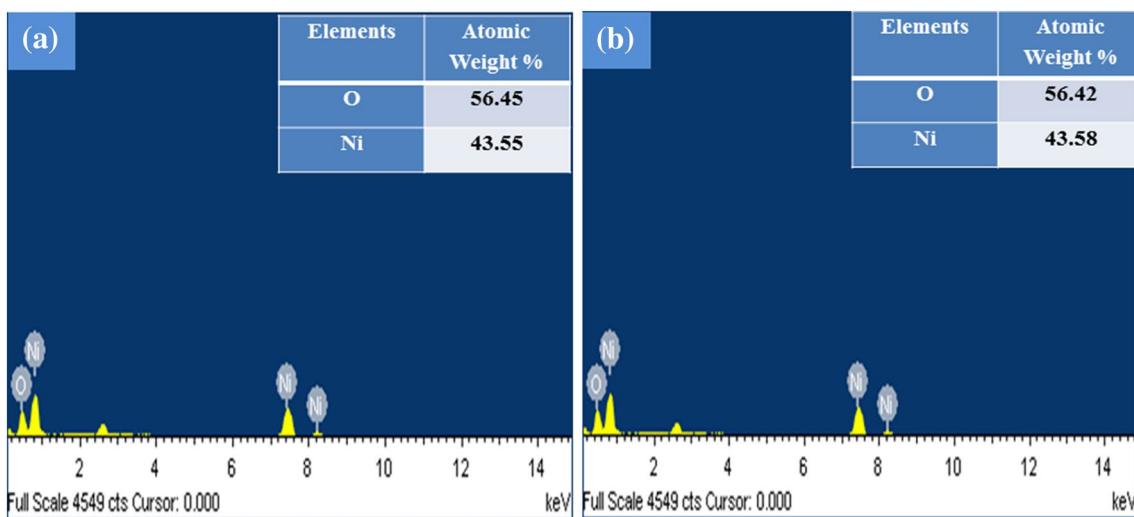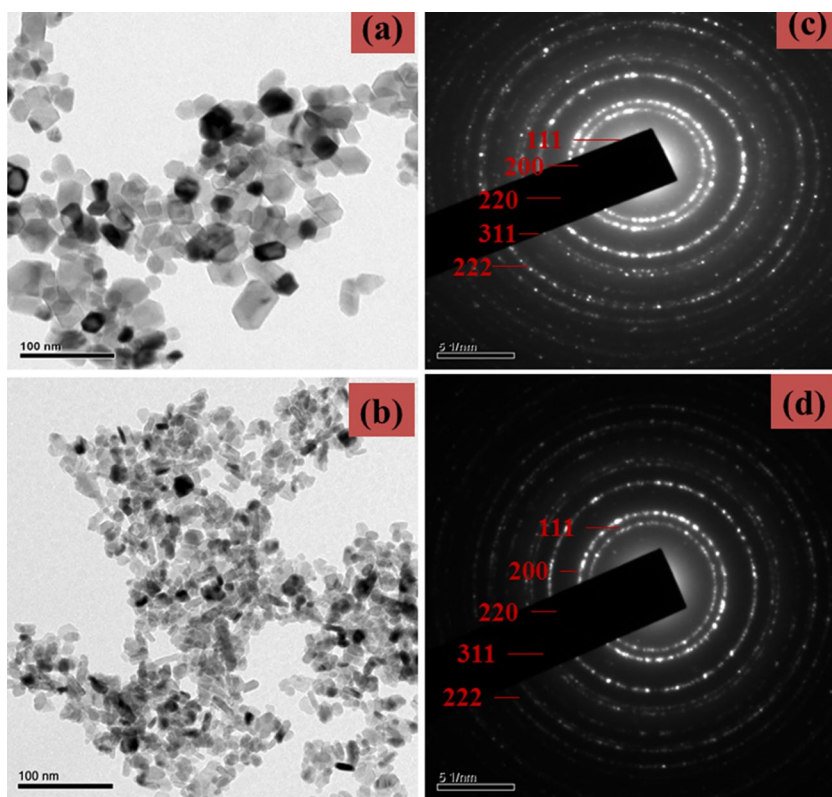

Fig. 4 EDAX spectra of **a** green synthesized NiO NPs and **b** chemically synthesised NiO NPs

of green and chemically synthesised NiO NPs annealed at 600 °C. The UV emission peak (K1) observed at 395, 396 (see Table 3) which correspond to a near band edge emission in all the samples due to direct recombination of the excitations through an exciton–exciton scattering. It can be attributed to the intrinsic transitions of exciton from the conduction band to the valance band, i.e., electronic transition involving $3d^8$ electrons of the Ni^{2+} ions

[24]. The violet emission peaks K2 and K3 appear at 418, 424, 438 and 440 nm for green and chemically synthesised NiO NPs. The analysis of the emission peaks (K5 and K6) appear at 449, 456 and 468 nm which correspond to the blue region with major irregularities. It is due to the oxygen vacancies; these vacancies are responsible for the increment in defect levels in the crystals and thus enhance the visible emission spectra [25]. The green

Fig. 5 UV–visible spectra of green and chemically synthesised NiO NPs
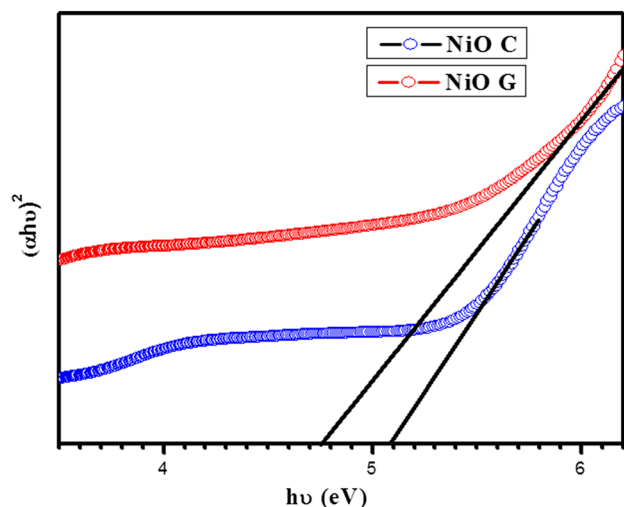
Fig. 6 Band gap spectra of green and chemically synthesised NiO NPs

emission peaks (K7) appear at 491 and 505 nm for green and chemically synthesised NiO NPs. Besides, it should be noted that the PL spectra in Fig. 7 do not show any yellow-green visible luminescence from the green and chemically synthesised NiO NPs. It confirmed that there is no Ni vacancies present in both green and chemically synthesised NiO NPs.

4.7 X-ray photoelectron spectroscopy (XPS) studies

The electronic structure and composition of the green and chemically synthesized NiO NPs are shown in Fig. 8a–c. Fig. 8a shows the XPS survey scan of green and chemically synthesised NiO NPs, which confirms the presence of Ni, O and C in the synthesized samples.

The asymmetric O (1s) signals are divided into three symmetrical signals (Fig. 8b), namely V1, V2 and V3 in the Gaussian fitting. The lower binding energy peak V1 at 529.17, 529.65 eV is from Ni^{2+} associated with the Ni–O octahedral bonding of cubic rock salt NiO [26–28]. The higher binding energy peak (V2) at 530.65 eV are attributed to Ni–O–Ni, whereas the peak (V3) at 532.40 eV is attributed to Ni–O–H at the surface of the NiO nanoparticles [29, 30], or it is related to a transition from O 1s states to the empty O-2p state hybridized with Ni-3d states.

The other peak noted for the binding energy at 535.39 eV is related to the empty O 2p states hybridized with Ni 4sp states [31, 32]. Chemical and green synthesized NiO nanoparticles samples show the positional shift in O (1s) spectra and lower binding energy values are given in Table 4.

Figure 8c shows the Cu (2p) core level binding energy spectrum of the green and chemically synthesized NiO nanoparticles. The two sharp peaks obtained at binding energies of 872.70 eV and 855.42 eV correspond to Ni 2p1/2 and Ni 2p3/2 while their satellite peaks due to shake-up process appear at about 879.32 eV and 861.57, 867.16 eV respectively [33]. The spin–orbit splitting between the Ni ($2p_{3/2}$) and Ni ($2p_{1/2}$) core level of NiO NPs is 17.28 eV and which is also agree with an earlier reports [34, 35]. The atomic percentage of Ni and O are calculated as 43.58% and 56.42% which reveals the presence of oxygen in excess of Ni. It shows that the particle is non-stoichiometric NiO which confirms the formation of Ni^{2+} vacancies.

4.8 Electron paramagnetic resonance studies

EPR spectroscopy is an useful technique for studying the materials with unpaired electrons and defects. In order to understand the effect of nanostructures, EPR measurement was carried out on the NiO NPs synthesised by chemical and green synthesis method. Figure 9 displays room temperature EPR spectra for two different synthesised NiO NPs. The calculated 'g' values of the samples are 2.250 and 2.214 for green and chemically synthesised NPs respectively. In addition, the Ni^{2+} ion in NiO has a g-value ~ 2.0. [36]. The relative intensity and line width of these absorption lines exhibit a strong dependence on different synthesis methods and solvents. The peak intensity increases significantly and the broad shift towards lower fields indicate
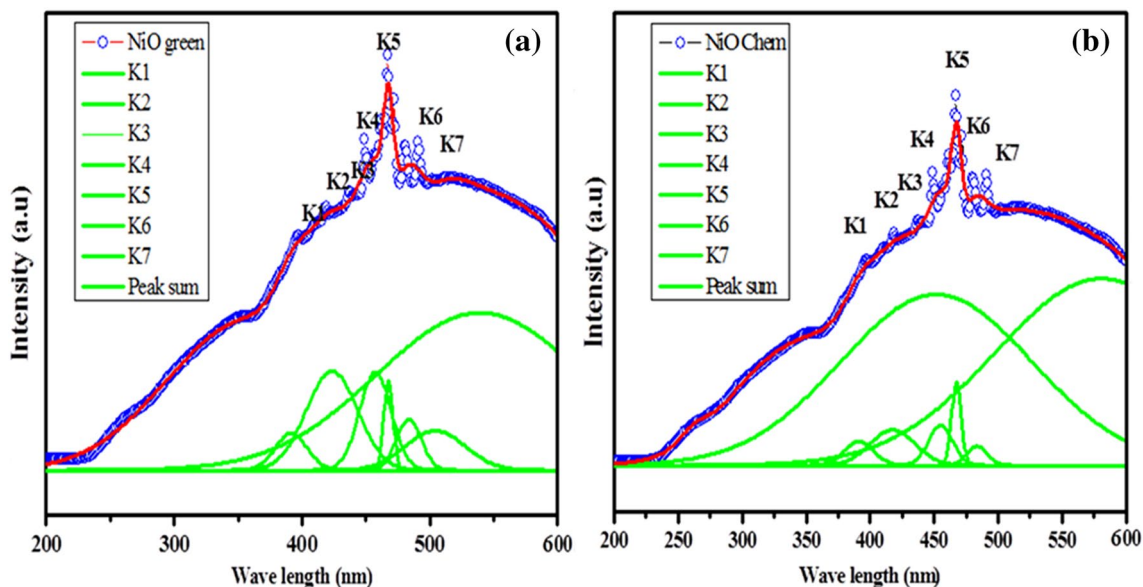
Fig. 7 Photoluminescence emission spectra of green and chemically synthesised NiO NPs

Table 3 Comparison of the PL emission values of the green and chemically synthesised NiO NPs

Peak name	NiO green (nm)	NiO chem (nm)	Assignment
K1	396	395	Near band edge
K2	424	418	Violet emission band
K3	440	438	Violet emission band
K4	456	449	Blue emission band
K5	468	468	Blue emission band
K6	484	480	Blue emission band
K7	505	491	Green emission band

a clear ferromagnetic signature of the both NiO materials. [37]. Thus, the enhanced intensity of EPR spectra and the larger g-value for the chemically synthesised NiO NPs may indicate the increasing amount of nickel vacancies.

4.9 Zeta potential distribution studies

Figure 10 depicts the zeta potential measurement of green and chemically synthesised NiO NPs. The zeta potential is a parameter widely used to predict colloidal suspension stability of synthesised NiO nanoparticles. It provides the degree of repulsion between similarly charged particles in dispersion medium. The greater stability of the nanoparticles is associated with its negative charge (i.e.) nanoparticles with more negative charge (< -30) showed a greater stability [38]. In the current study, the zeta potential values
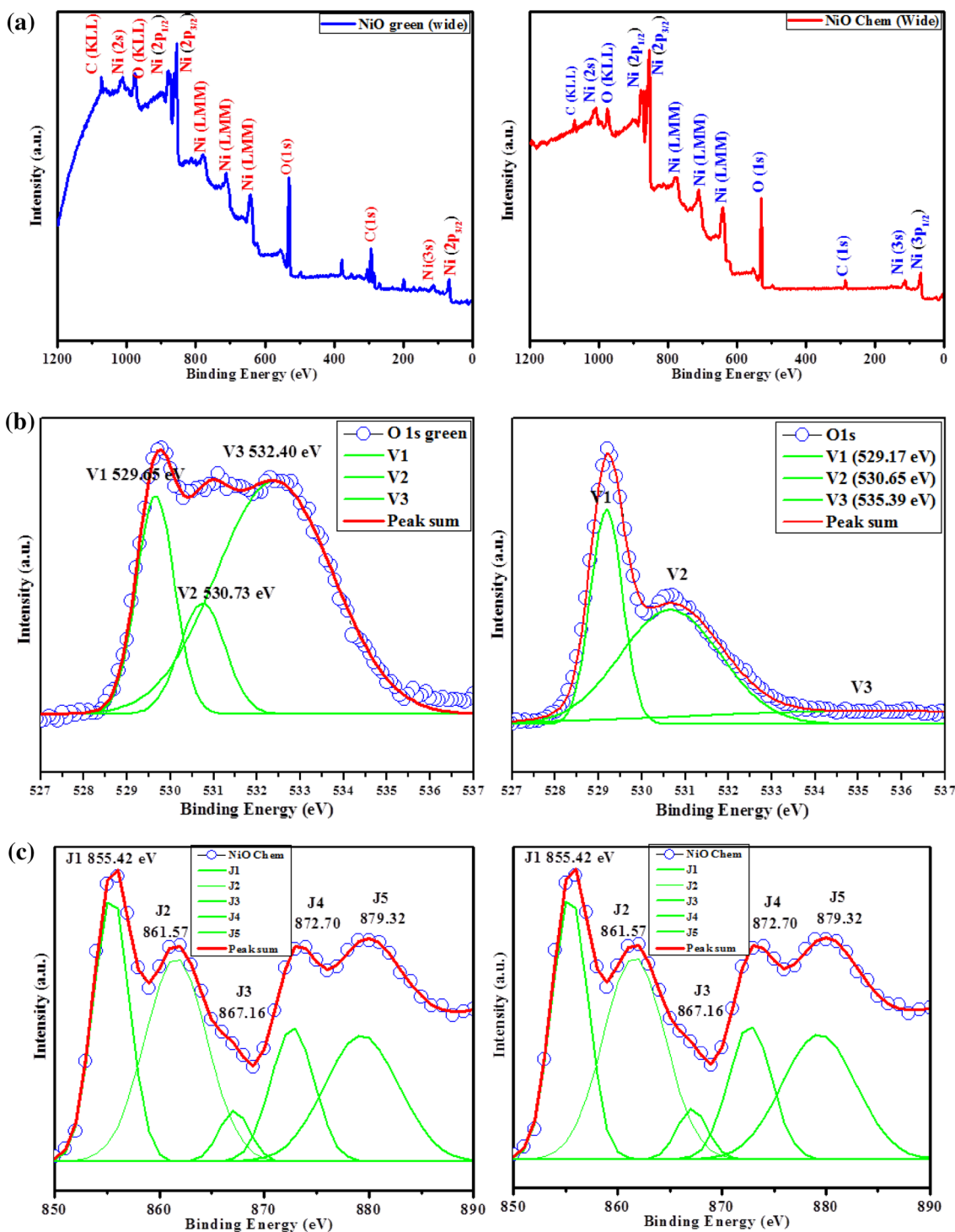
of green and chemically synthesised NiO NPs are -6.05 and -17.9 mV respectively. This result reveals that the chemically synthesised NiO NPs is moderately stable than that of the green synthesised NiO NPs.

5 Microbial toxicity studies

Figure 11 exhibits the zone of inhibition of green and chemically synthesised NiO nanoparticles at different concentrations (1, 3, 5 mg/ml) against *S. aureus* (gram positive) and *E. coli* (gram negative) bacterial pathogens. Figure 11a–d shows the size of the zone of inhibition and antibacterial action of both NiO NPs loaded with test samples. It is clear from Table 5, that the chemically synthesised NiO nanoparticles have shown effective antibacterial activities against all the pathogens. It is also observed that the green and chemically synthesized NiO nanoparticle was effective over Gram positive *S. aureus* showing a large value of zone of inhibition than the gram negative bacterial pathogens. This observation reveals the greater resistance or tolerance of gram negative pathogens over gram positive bacterial strains. The reactivity of the nanoparticles with bacterial cell depends not only on the metal oxide employed but also on the bacterial species tested [39].

Antibacterial activity of the nanoparticles depends on the particle size, stability and the concentration of the growth medium. As the outer cellular membrane of the bacterial strains is of nanoscale pores, there lies a better reactivity of the nanoparticle with that of the pathogens.
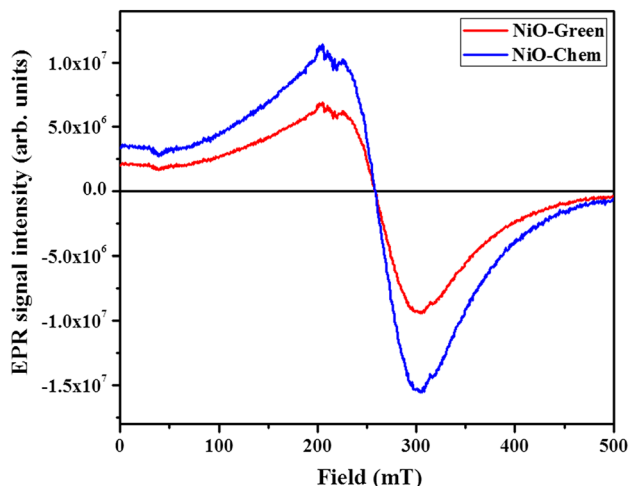
Fig. 8 XPS spectra of the green and chemically synthesised NiO NPs. **a** Survey scan, **b** O 1s spectrum, **c** Ni 2p spectrum

The green and chemically synthesised NiO nanoparticles have a particle size of 13 nm, 27 nm and it is better proven through the obtained XRD and HRTEM results. Particle size has a significant role over the antibacterial activity and most of the studies have proven that the

antibacterial activity increases with the decreasing particle size [40–42]. As both the green and chemically synthesized NiO nanoparticle has less particle size, it gains the tendency to attach to the cell membrane by electrostatic interaction [43] and trigger the initiation of the oxidative
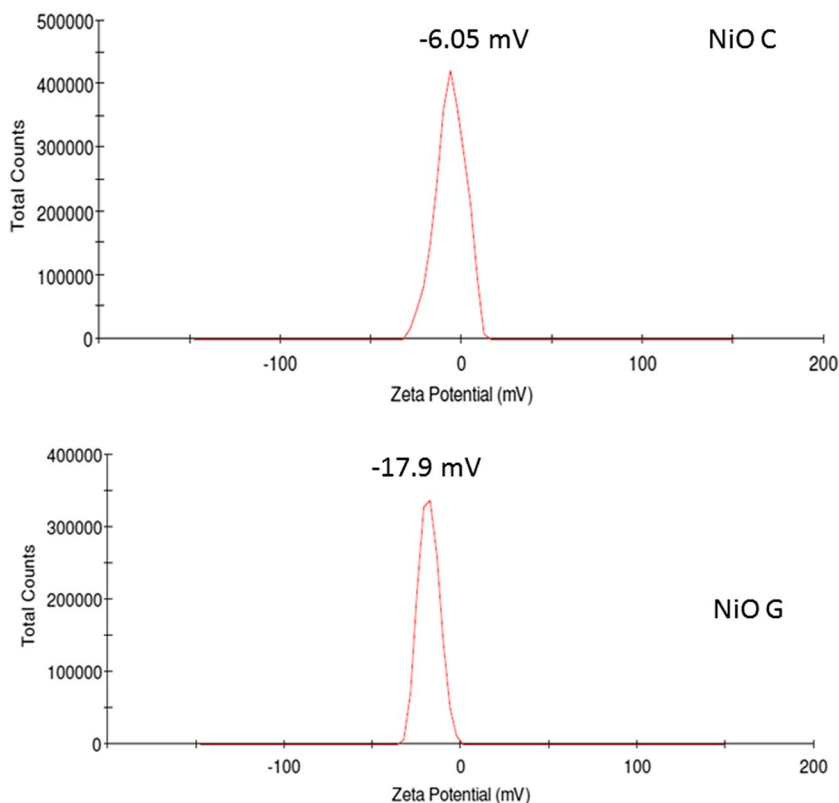
Table 4 Comparison of the XPS binding energy values of the green and chemically synthesised NiO NPs

Sample	Ni (2p) in eV		O (1s) in eV		
	Ni (2p$_{3/2}$)	Ni (2p$_{1/2}$)	V1	V2	V3
NiO green	855.42	872.70	529.85	531.31	533.97
NiO chem	855.42	872.70	529.79	531.27	532.31

Fig. 9 EPR spectra of green and chemically synthesised NiO NPs

stress, thus resulting in free radical formation ROS, which disrupts the bacterial cell membrane as shown in Fig. 11. Production of ROS depends on the electronic structure of the metal oxides and the redox potentials of ROS generation reactions [44, 45]. The high antibacterial activity of the nanoparticles may be attributed to their definite chemical composition, particle size, tendency to release the metal ions and morphology, thereby inducing the trans membrane electron transfer, penetration and oxidization of cell components and production of secondary products (ROS), which results in cell damage. The précised toxicity mechanism of the metal oxide nanoparticle against various bacteria is not clearly understood. The governing mechanism for the antibacterial activity of the synthesized NiO nanoparticle maybe due to the electrostatic interaction between the positively charged nickel ions and the negatively charged bacterial cell membranes, which is in agreement with the studies of Basak et al. [46]. The release of nickel ion (Ni^{2+}), from the NiO nanoparticles penetrate into the cell wall causing damage in the DNA, protein, mitochondria and also disturb in the electron transport resulting in cell death. Diffusion and accumulation of NiO NPs in the cell membrane and changes the membrane permeability with subsequent protein leakage [47, 48]. Another possible mechanism is represented below.
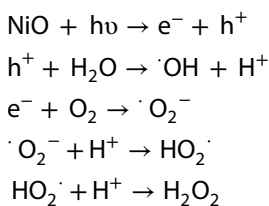
Fig. 10 Zeta potential measurement of green and chemically synthesised NiO NPs

Fig. 11 Size of the zone of inhibition formed around each disc, loaded with test samples, indicating the antibacterial activity. **a**, **b** Green synthesised NiO NPs, **c**, **d** chemically synthesised NiO NPs against G+ and G− bacterial strains
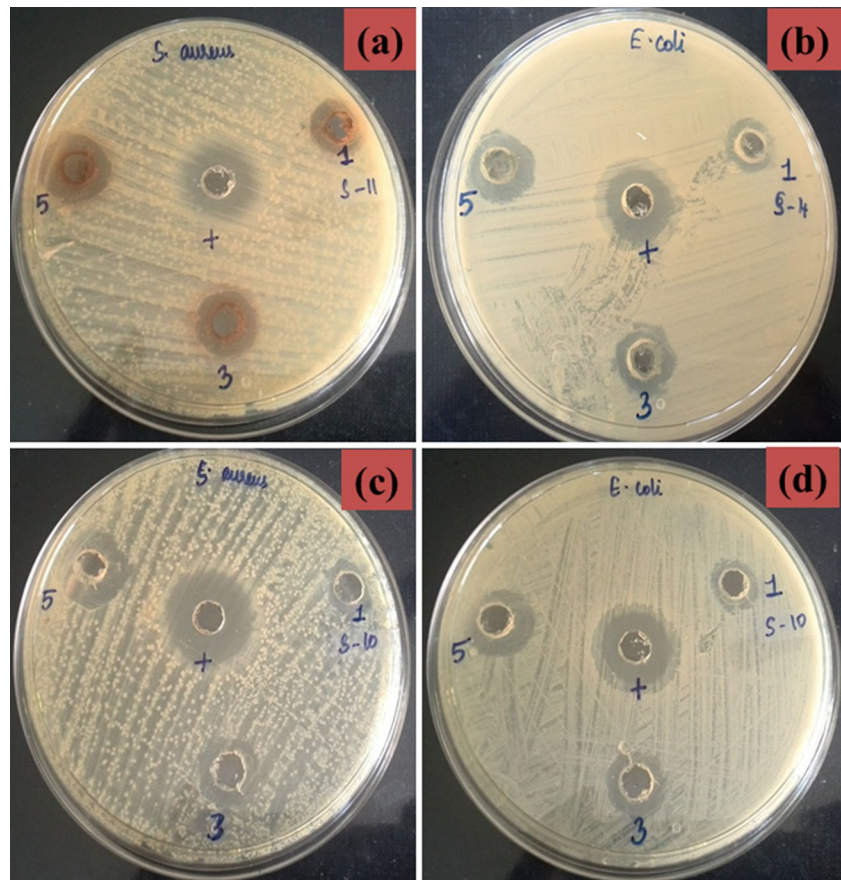
Table 5 Zone of inhibition value of green and chemically synthesised NiO NPs treated with micro organism [46–48]

Sample code	Zone of inhibition (mm)				
	Micro organism	Control (10 µg/ml)	1 mg/ml	3 mg/ml	5 mg/ml
NiO (green)	S. aureus	16	5	8	12
	E. coli	15	3	6	11
NiO (chem)	S. aureus	19	6	11	17
	E. coli	18	5	9	15

$$NiO + h\upsilon \rightarrow e^- + h^+$$

$$h^+ + H_2O \rightarrow {}^{\cdot}OH + H^+$$

$$e^- + O_2 \rightarrow {}^{\cdot}O_2{}^-$$

$${}^{\cdot}O_2{}^- + H^+ \rightarrow HO_2{}^{\cdot}$$

$$HO_2{}^{\cdot} + H^+ \rightarrow H_2O_2$$

When the band gap E_g is less than that of the incident photon energy, photo excitation takes place with the generation of holes (h^+) in the valence band and electrons (e^-) in the conduction band. These photo excited holes and electrons having high oxidizing and reducing properties, further react with donor (water and hydroxyl ions) and acceptor (molecular oxygen) and results in the production of different reactive oxygen species (ROS). The excited electron traps the molecular oxygen to generate superoxide anion (O^{2-}), which further reacts with free water molecules to form hydrogen peroxide ($H_2O_2^{\cdot}$), a powerful oxidizing agent. The holes absorb electrons from water and hydroxyl ions to form hydroxyl radicals (${}^{\cdot}OH$), and these reactive oxygen species generated are responsible for the damage of cell membrane, DNA and protein [49–51].

In the present study, XRD and HRTEM results reveals that there is a decrease in the particle size for chemically synthesised NiO NPs when compared to the green synthesised NiO NPs. EPR, PL and XPS studies confirmed that highest oxygen and Ni vacancies are present in the chemically synthesised NiO NPs and it produced more ROS in cell membrane. In this aforementioned mechanism and studies reveal that the chemically synthesised NiO NPs possess more microbial toxicity than that of the green synthesised NiO NPs.
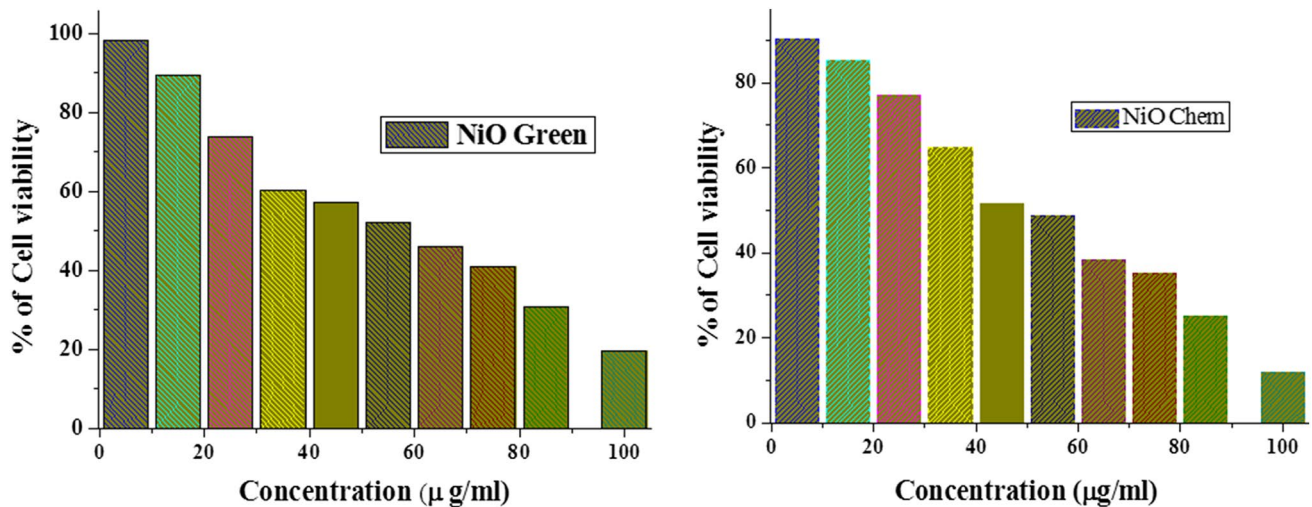
Fig. 12 In vitro cytotoxicity of green and chemically synthesised NiO NPs against MCF-7 cells

6 In vitro cytotoxicity studies on MCF-7 cells

Because nanoparticles of different origin have diverse physicochemical characteristics, their biological responses and subsequent mechanisms will produce dissimilar cytotoxic effects. A thorough characterisation and identification of the important physicochemical properties on the different mechanisms of cytotoxicity require a broad range of cytotoxicity assays. This thesis will present two different cytotoxicity assays; MTT and acridine orange/ethidium bromide staining.

6.1 MTT assay

The cytotoxic effect of the green and chemically synthesized NiO NPs are examined on cultured MCF-7 human breast cancer cells by exposing cells for 24 h to medium containing the NiO NPs at 5–100 μg/ml concentrations (Fig. 12). In the present studies, the results reveal that MCF 7 cells respond to NiO NPs with dose dependent concentrations with increased cytotoxicity. The green synthesised NiO NPs at lower concentration (5 μg/ml) showed 98% cell viability and 92% of cell viability is shown in chemically synthesised NiO NPs respectively. The cell viability was decreased up to 22% for green synthesised NiO NPs and 15% for chemically synthesised NiO NPs at higher concentration (100 μg/ml). The half maximum inhibitory concentration (IC_{50}) of green and chemically synthesised NiO NPs against MCF-7 cells was found to be 55 and 45 μg/ml respectively. IC_{50} value of the green and chemically synthesised NiO NPs are presented in Fig. 12. From these results, it is confirmed that the chemically synthesised NiO NPs possess highest cytotoxicity effects than that of the green synthesised NiO NPs.

6.2 Fluorescence microscopic analysis of apoptotic cell death (AO and EB staining)

AO/EB staining adopting fluorescence microscopy also revealed apoptosis from the perspective of fluorescence. The MCF-7 cancer cells were exposed to the concentrations of green and chemically synthesised NiO NPs for 24 h. In this study, we used acridine orange/ethidium bromide (AO/EB) double staining assay [52]. Acridine orange is taken up by both viable and nonviable cells and emits green fluorescence if interrelated into double stranded nucleic acid (DNA). An Ethidium bromide is taken up only by the nonviable cells and emits red fluorescence by intercalation into DNA.

Apoptotic cells have orange to red nuclei with condensed or fragmented chromatin. Necrotic cells have an uniformly orange to red nuclei with condensed structure. As shown in Fig. 13a–c, the nuclei of untreated normal cells are stained green and showed normal structure, while NiO NPs treated cells are stained red and orange, representing the hallmark of apoptosis. Figure 13b, c exhibited the morphological alteration of MCF-7 cells treated with green and chemically synthesised NiO NPs with IC_{50} concentrations after staining with AO/EB.

Our results confirmed that NiO NPs induced apoptosis at the concentrations evaluated, in agreement with the cytotoxic results. The chemically synthesised NiO NPs possess highest apoptosis morphology as compared to green synthesised NiO NPs. This is due to their smaller size and large surface area which is generally causes the production of ROS.

Fig. 13 Cells were treated NiO with IC_{50} concentrations and the morphological changes were observed using a fluorescent microscope after staining with AO/EB for **a** control, **b** chemically synthesized NiO NPs and **c** green synthesized NiO NPs
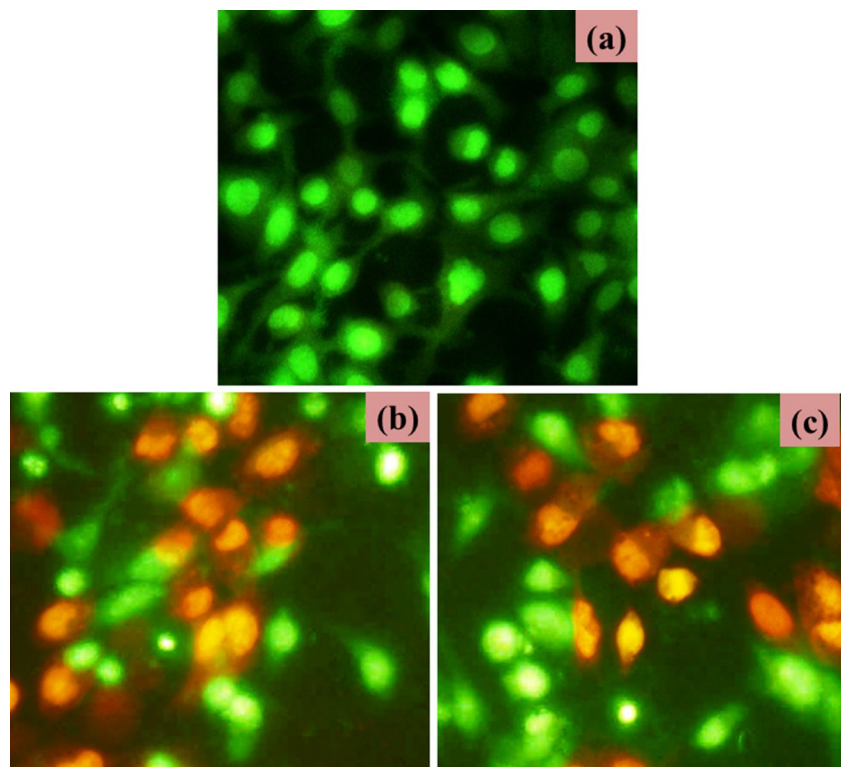
7 Conclusion

NiO NPs were successfully synthesized by green and co-precipitation method. The *G. sylvestre* plant extract has been used as a potential reducing agent for the synthesis of NiO NPs which was confirmed by XRD studies. The cubic structure was identified for green and chemically synthesised NiO NPs through XRD analysis. The presence of all functional groups was ascertained from FTIR analysis. Cube shaped morphologies were found in both NiO NPs observed from HRTEM analysis. EDAX analysis has confirmed the presence of Ni and O in NiO NPs synthesised through both the methods. The XPS studies showed that from the indexed peaks corresponding to O (1*s*), Ni (2*p*), the respective binding energies of the elements were estimated. The PL emission studies showed that the chemically synthesised NiO NPs altered the band emission, which is due to oxygen vacancies and surface defects. An EPR study has confirmed the ferro magnetic in nature and also Ni vacancies present in the samples. Moderate zeta potential values were observed in green and chemically synthesised NiO NPs.

The potential microbial and MCF-7 cancer cell line toxicity were evaluated for green and chemically synthesised NiO NPs. Chemically synthesised NiO NPs have highest toxicity than green synthesised NiO NPs. With reference to cell death, a minimum concentration of 45 μg/ml for chemically synthesised NiO NPs was well enough to induce 50% cell mortality as compared to green synthesised NiO NPs (55 μg/ml). In the chemically synthesised NiO NPs, the wavelength of the blue green was greater than the green synthesised NiO NPs. This showed an increased number of oxygen vacancies and interstitial oxygen vacancies in the chemically synthesised NiO NPs, leading to a higher number of ROS as compared to that of the green synthesised NiO NPs. The mode of cell death was assessed through adopting an AO and EB staining. The chemically synthesised NiO NPs induced higher percentage of apoptosis than necrosis as compared to green synthesised NiO NPs. The green synthesised NiO NPs exhibit lowest toxicity and environmental friendly when compared chemically synthesised NiO NPs.

Compliance with ethical standards

Conflict of interest The authors declare that they have no conflict of interest.

References

1. Hussain SM, Javorina AK, Schrand AM, Duhart HM, Ali SF, Schlager JJ (2006) The interaction of manganese nanoparticles with PC-12 cells induces dopamine depletion. Toxicol Sci 92(2):456–463

2. Singh N, Manshian B, Jenkins GJ, Griffiths SM, Wiiliams PM, Maffeis TG, Wright CJ, Doak SH (2009) Nanogenotoxicology: the DNA damaging potential of engineered nanomaterials. Biomaterials 30(23–24):3891–3894

3. Muller J, Huaux F, Moreau N, Misson P, Heilier JF, Delos M, Arras M, Fonseca A, Nagy JB, Lison D (2005) Respiratory toxicity of multi-wall carbon nanotubes. Toxicol Appl Pharmacol 207(3):221–231

4. Oberdörster G (2001) Pulmonary effects of inhaled ultrafine particles. Int Arch Occup Environ Health 74(1):1–8

5. Li M, Pokhrel S, Jin X, Mädler L, Damoiseaux R, Hoek EM (2011) Stability, bioavailability and bacterial toxicity of ZnO and iron-doped ZnO nanoparticles in aquatic media. Environ Sci Technol 45(2):755–761

6. Rosi NL, Mirkin CA (2005) Nanostructures in biodiagnostics. Chem Rev 105(4):1547–1562

7. Dunnick JK, Benson JM, Hobbs CH, Hahn FF, Cheng YS, Edison AF (1988) Comparative toxicity of nickel oxide, nickel sulfate hexahydrate and nickel subsulfide after 12 days of inhalation exposure to F344/N rats and B6C3F$_1$ mice. Toxicology 50(2):145–156

8. Benson JM, Henderson RF, McClellan RO (1986) Comparative cytotoxicity of four nickel compounds to canine and rodent alveolar macrophages *in vitro*. J Toxicol Environ Health 19(1):105–110

9. Mariam AA, Kashif M, Arokiyaraj S, Bououdina M, Sankaracharyulu MGV, Jayachandran M, Hashim U (2014) Bio-synthesis of NiO and Ni nanoparticles and their characterization. Dig J Nanomater Biostructures 9(3):1007–1019

10. Adam K, Turk M, Oguztuzun S, Kiic M, Demirel M, Tandogan N, Ersayar E, Latif O (2010) Cytotoxicity and apoptotic effects of nickel oxide nanoparticles in cultured HeLa cells. Folia Histochem Cytobiol 48(4):524–529

11. Ahamed M, Ali D, Alhadlaq HA, Akhtar MJ (2013) Nickel oxide nanoparticles exert cytotoxicity via oxidative stress and induce apoptotic response in human liver cells (HepG2). Chemosphere 93(10):2514–2522

12. Duan WX, He MD, Mao L, Qian FH, Li YM, Pi HF, Liu C, Chen CH, Lu YH, Cao ZW, Zhang L, Yu ZP, Zhou Z (2015) NiO nanoparticles induce apoptosis through repressing SIRT1 in human bronchial epithelial cells. Toxicol Appl Pharmacol 286(2):80–91

13. Ramasami AK, Reddy MV, Balakrishna GR (2015) Combustion synthesis and characterization of NiO nanoparticles. Mater Sci Semicond Process 40:194–202

14. Talebian N, Doudi M, Kheiri M (2014) The anti-adherence and bactericidal activity of sol–gel derived nickel oxide nanostructure films: solvent effect. J Sol Gel Sci Technol 69(1):172–182

15. Dhawan A, Sharma V (2010) Toxicity assessment of nanomaterials: methods and challenges. Anal Bioanal Chem 398(2):589–605

16. Wright GD (2000) Resisting resistance: new chemical strategies for battling superbugs. Cell Chem Biol 7(6):127–132

17. Mosmann T (1983) Rapid colorimetric assay for cellular growth and survival: application to proliferation and cytotoxicity assays. J Immunol Methods 65(1–2):55–63

18. Spector DL, Goldman RD, Leinwand LA (1998) Culture and biochemical analysis of cells. Cell Lab Man 1:341–349

19. Song X, Gao L (2008) Facile synthesis of polycrystalline NiO nanorods assisted by microwave heating. J Am Ceram Soc 91(10):3465–3468

20. Wang Y, Zhu J, Yang X, Lu L, Wang X (2005) Preparation of NiO nanoparticles and their catalytic activity in the thermal decomposition of ammonium perchlorate. Thermochim Acta 437(1–2):106–109

21. Kumar V, Som S, Kumar V, Ntwaeaborwa OM, Coetsee E, Swart HC (2014) Tunable and white emission from ZnO: Tb^{3+} nanophosphors for solid state lighting applications. Chem Eng J 255:541–552

22. Yamamoto H, Tanaka S, Hirao K (2003) Effects of substrate temperature on nanostructure and band structure of sputtered Co$_3$O$_4$ thin films. J Appl Phys 93(7):4159–4162

23. Soriano L, Abbate M, Fernandez A, Gonzalez-Elipe AR, Sanz JM (2003) The electronic structure of mesoscopic NiO particles. Chem Phys Lett 208(5–6):460–463

24. Anandan K, Rajendran V (2011) Morphological and size effects of NiO nanoparticles via solvothermal process and their optical properties. Mater Sci Semicond Process 14(1):43–47

25. Jain S, Khare PS, Pandey DK (2016) Synthesis and analysis of photoluminescence properties of In and Sn doped nickel oxide powders. Optik 127(16):6763–6767

26. Ratcliff EL, Meyer J, Steirer KX, Garcia A, Berry JJ, Ginley DS, Olson DC, Kahn A, Armstrong NR (2011) Evidence for near-surface NiOOH species in solution-processed NiO$_x$ selective interlayer materials: impact on energetics and the performance of polymer bulk heterojunction photovoltaics. Chem Mater 23(22):4988–5000

27. Uhlenbrock S, Scharfschwerdt C, Neumann M, Illing G, Freund HJ (1992) The influence of defects on the Ni 2p and O 1s XPS of NiO. J Phys Condens Matter 4:7973–7978

28. Kim KS, Winograd N (1974) X-ray photoelectron spectroscopic studies of nickel–oxygen surfaces using oxygen and argon ion bombardment. Surf Sci 43(2):625–643

29. Kim SI, Lee JS, Ahn HJ, Song HK, Jang JH (2013) Facile route to an efficient NiO super capacitor with a three-dimensional nano network morphology. ACS Appl Mater Interfaces 5(5):1596–1603

30. Salvati L, Makovsky LE, Stencel JM, Brown FR, Hercules DM (1981) Surface spectroscopic study of tungsten–alumina catalysts using X-ray photoelectron, ion scattering, and Raman spectroscopies. J Phys Chem 85:3700–3707

31. Mossanek RJO, Niizares GD, Gutierrez A, Abbate M, Dyaz-Fernandez D, Oriano L (2013) Effects of Ni vacancies and crystallite size on the O 1s and Ni 2p X-ray absorption spectra of nanocrystalline NiO. J Phys Condens Matter 25(49):495–506

32. Soriano L, Gutirrez A, Preda I, Palacn S, Abbate JMSM, Trigo JF, Vollmer A, Bressler P (2006) Splitting of Ni 3d states at the surface of NiO nanostructures. Phys Rev B 74(19):193402

33. Biju V (2007) Ni 2p X-ray photoelectron spectroscopy study of nanostructured nickel oxide. Mater Res Bull 42(5):791–796

34. Kumar H, Ghosh S, Avasthi DK, Kabiraj D, Lalla NP, Shripathi T, Pivin JC (2010) Magnetic and field emission studies of atom beam sputtered Ni:SiO$_2$ granular films. Vacuum 85(2):139–144

35. Lenglet M, Hochu F, Dürr J, Tuilier MH (1997) Investigation of the chemical bonding in 3d8 nickel (II) charge transfer insulators (NiO, oxidic spinels) from ligand-field spectroscopy, Ni 2p XPS and X-ray absorption spectroscopy. Solid State Commun 104(12):793–798

36. Rubinsteina M, Kodamab RH, Makhlouf SA (2001) Electron spin resonance study of NiO antiferromagnetic nanoparticles. J Magn Magn Mater 234(2):289–293

37. Srinivas K, Rao SM, Reddy PV (2011) Structural, electronic and magnetic properties of Sn$_{0.95}$Ni$_{0.05}$O$_2$ nanorods. Nanoscale 3(2):642–653

38. Garcia AB, Guesta A, Montes-Moran MA, Martinez-Alonso A, Tascon JMD (1997) Zeta potential as a tool to characterize

plasma oxidation of carbon fibers. J Colloid Interface Sci 192(2):363–367

39. Hassen A, Saidi N, Cherif M, Boudabous A (1998) Effects of heavy metals on *Pseudomonas aeruginosa* and *Bacillus thuringiensis*. Bioresour Technol 65(1–2):73–82

40. Nel A, Xia T, Madler L, Li N (2006) Toxic potential of materials at the nanolevel. Science 311(5761):622–627

41. Jiang W, Mashayekhi H, Xing B (2009) Bacterial toxicity comparison between nano and micro-scaled oxide particles. Environ Pollut 157(5):1619–1625

42. Simon-Deckers A, Loo S, Mayne-L'hermite M, Herlin-Boime N, Menguy N, Reynaud C, Gouget B, Carriére M (2009) Size, composition and shape dependent toxicological impact of metal oxide nanoparticles and carbon nanotubes toward bacteria. Environ Sci Technol 43(21):8423–8429

43. Thill A, Zeyons O, Spalla O, Chauvat F, Rose J, Auffan M, Flank AM (2006) Cytotoxicity of CeO_2 nanoparticles for *Escherichia coli*: physico-chemical insight of the cytotoxicity mechanism. Environ Sci Technol 40(19):6151–6156

44. Gratzel M (2001) Photo electrochemical cells. Nature 414(6861):338–344

45. Ireland JC, Klostermann P, Rice E, Clark R (1993) Inactivation of *Escherichia coli* by titanium dioxide photocatalytic oxidation. Appl Environ Microbiol 59(5):1668–1670

46. Basak G, Das D, Das N (2014) Dual role of acidic diacetate sophorolipid as bio stabilizer for ZnO nanoparticle synthesis and bio functionalizing agent against *Salmonella enterica* and *Candida albicans*. J Microbiol Biotechnol 24(1):87–96

47. Wong KKY, Liu X (2010) Silver nanoparticles—the real 'silver bullet' in clinical medicine. Med Chem Comm 1(2):125–131

48. Baek YW, An YJ (2011) Microbial toxicity of metal oxide nanoparticles (NiO, ZnO and Sb_2O_3) to *Escherichia coli*, *Bacillus subtilis* and *Streptococcus aureus*. Sci Total Environ 409(8):1603–1608

49. Du J, Gebicki JM (2004) Proteins are major initial cell targets of hydroxyl free radicals. Int J Biochem Cell Biol 36(11):2334–2343

50. Xia T, Kovochich M, Brant J, Hotze M, Sempf J, Oberley T, Sioutas C, Yeh JI, Wiesner MR, Nel AE (2006) Comparison of the abilities of ambient and manufactured nanoparticles to induce cellular toxicity according to an oxidative stress paradigm. Nano Lett 6(8):1794–1807

51. Burello E, Worth AP (2011) A theoretical framework for predicting the oxidative stress potential of oxide nanoparticles. Nanotoxicology 5(2):228–235

52. Baskic D, Popovic S, Ristic P, Arsenijevic NN (2006) Analysis of cycloheximide-induced apoptosis in human leukocytes: fluorescence microscopy using annexin-V/propidium iodide versus acridine orange/ethidium bromide. Cell Biol Int 30(11):924–932